

Model Predictive Direct Current Control for a Grid-Connected Converter: LCL -Filter versus L -Filter

James Scoltock¹, Tobias Geyer², and Udaya Madawala¹

¹Department of Electrical and Computer Engineering, The University of Auckland, 1010 Auckland, New Zealand.
Email: jsco075@aucklanduni.ac.nz, u.madawala@auckland.ac.nz

²ABB Corporate Research, 5405 Baden-Dättwil, Switzerland. Email: t.geyer@ieee.org

Abstract—This paper presents a modified Model Predictive Direct Current Control (MPDCC) strategy for use with a Neutral Point Clamped (NPC) converter connected to the grid via an LCL -filter. The modified MPDCC strategy incorporates an Active Damping (AD) scheme based on the Virtual Resistor (VR) concept, which suppresses spectral content around the resonant frequency of the LCL -filter, enabling low levels of grid current distortion to be achieved with low switching frequencies. Through simulation the proposed scheme is compared against conventional MPDCC with a direct connection to the grid (L -filter). By comparing the trade-off curves of grid current distortion against device switching losses, it is shown that the performance of the proposed strategy is superior to that of conventional MPDCC with a direct grid-connection across a range of operating points.

Index Terms—Active damping, direct current control, grid connected converter, LCL -filter, model predictive control

I. INTRODUCTION

Recently, Model Predictive Control (MPC) has gained popularity within the power electronics and drives community as a promising alternative to traditional control and modulation strategies. MPC is of particular interest in Medium-Voltage (MV) applications, as it has the potential to reduce converter switching frequency and losses whilst maintaining acceptable levels of output distortion, or vice versa. Model Predictive Direct Current Control (MPDCC) [1], [2], which was originally developed for induction machine drives, is a variant of MPC which is well suited to grid-connected applications, where the regulation of the line currents is often the main control objective.

LCL -filters are commonly used to interface converters with the grid, as they improve upon the harmonic attenuation offered by direct grid-connection (L -filters). The use of such filters, however, introduces additional challenges to controlling the line currents. Because the filter capacitance introduces a delay between the converter and the grid, it is difficult to directly control the grid-side currents, with system stability being a major concern [3] - [5]. Moreover, the resonance which is introduced by the filter needs to be adequately damped, using either a passive damping component(s) or an Active Damping (AD) strategy [6], [7]. If the resonant frequency is not adequately damped, then the introduction of an LCL -filter may worsen the performance of the system due to increased grid current distortion.

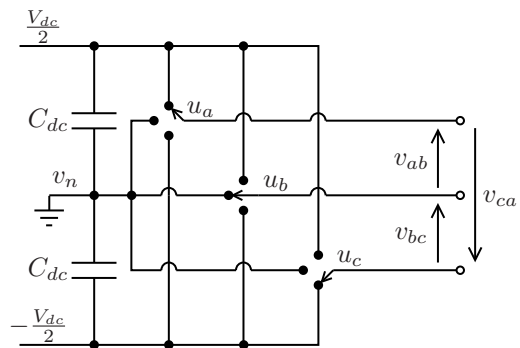


Fig. 1: Representation of a three-phase NPC converter.

This paper outlines a modified MPDCC strategy for use with a three-phase grid-connected Neutral Point Clamped (NPC) converter with an LCL -filter. The proposed scheme incorporates an AD strategy which is based on the Virtual Resistor (VR) concept, which emulates the effect of a physical damping resistor by modifying the current references with an additive damping quantity. The proposed strategy is evaluated through MATLAB-based simulation. In order to gauge the effectiveness of the proposed strategy, it is benchmarked against conventional MPDCC with an L -filter. The comparison is based on trade-off curves of grid current distortion against device switching losses, which allows a wide-range of steady-state operating points to be compared.

II. SYSTEM MODELLING

A. System Overview

A representation of a three-phase NPC converter is shown in Fig. 1. The three-phase filters which are used to interface the converter with the grid are shown in Figs. 2(a) and 2(b), where the input (converter) voltages are referred to the converter neutral point, v_n . In both cases, the grid impedance and transformer leakage inductance (where applicable) contribute to the grid-side inductance.

All modelling and simulation of the system is based on the assumption that the direction of current flow is from converter to grid and that the converter is fed from an ideal energy source, meaning that the DC-link voltage, V_{dc} , is constant.

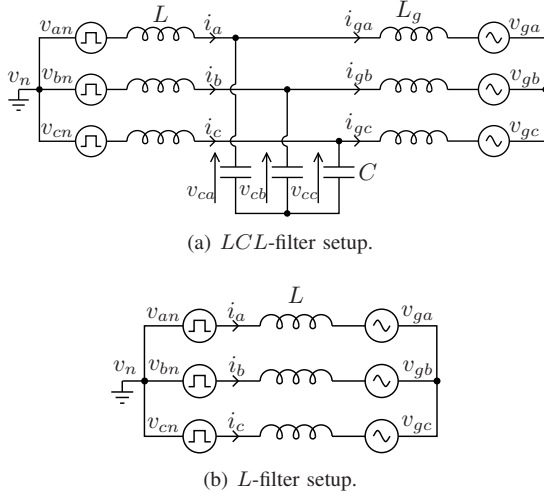


Fig. 2: Representation of three-phase grid-connection setups.

B. $\alpha\beta$ Reference Frame

Variables $\xi_{abc} = [\xi_a \ \xi_b \ \xi_c]^T$ in the three-phase abc reference frame are transformed to $\xi_{\alpha\beta} = [\xi_\alpha \ \xi_\beta]^T$ in the orthogonal $\alpha\beta$ reference frame through

$$\xi_{\alpha\beta} = \frac{2}{3}P\xi_{abc} \quad (1)$$

where P is the transformation matrix

$$P = \begin{bmatrix} 1 & -\frac{1}{2} & -\frac{1}{2} \\ 0 & \frac{\sqrt{3}}{2} & -\frac{\sqrt{3}}{2} \end{bmatrix} \quad (2)$$

It should be noted that (1) and (2) ignore the common-mode component of ξ_{abc} .

C. Converter Model

Each phase leg of the converter is able to assume one of three states, which are represented by the integer variables $u_a, u_b, u_c \in \{-1, 0, 1\}$. This gives rise to 27 possible switching states of the form $u_{abc} = [u_a \ u_b \ u_c]^T$. By transforming the switching states from the three-phase abc -frame to the orthogonal $\alpha\beta$ -frame, 19 distinct vectors of the form $u_{\alpha\beta} = [u_\alpha \ u_\beta]^T$ are yielded. The $\alpha\beta$ voltages as they appear across the output of the converter are subsequently given by

$$v_i = \frac{V_{dc}}{2}u_{\alpha\beta} \quad (3)$$

where $v_i = [v_{i\alpha} \ v_{i\beta}]^T$. In the converter considered, all switching transitions are allowed except for those which involve switching between the upper and lower rails. For example, a transition from $u_{abc} = [1 \ 1 \ 1]^T$ to $[0 \ 0 \ 1]^T$ is allowed, whereas a transition to $[-1 \ 1 \ 1]^T$ is not.

The neutral point potential, v_n , is affected when current is directly drawn from it when one or more of the switching states is zero. Assuming that $i_a + i_b + i_c = 0$, it follows that

$$\frac{dv_n}{dt} = \frac{1}{2C_{dc}}|u_{abc}|^T i_{abc} \quad (4)$$

where $|u_{abc}| = [|u_a| \ |u_b| \ |u_c|]^T$ and $i_{abc} = [i_a \ i_b \ i_c]^T$.

D. LCL-Filter Model

A state-space model which expresses the dynamics of the LCL -filter on a per-phase basis is required. With the filter modelled in the $\alpha\beta$ reference frame and with the filter states defined as the converter current, grid current, capacitor voltage and grid voltage, the state vector can be expressed as

$$x_1 = [i^T \ i_g^T \ v_c^T \ v_g^T]^T \quad (5)$$

with the converter current $i = [i_\alpha \ i_\beta]^T$, the grid current $i_g = [i_{g\alpha} \ i_{g\beta}]^T$, the capacitor voltage $v_c = [v_{c\alpha} \ v_{c\beta}]^T$ and the grid voltage $v_g = [v_{g\alpha} \ v_{g\beta}]^T$. With the input vector defined as the converter voltage v_i and the output vector defined as the converter current $y_1 = i$, the continuous-time state and output equations of the LCL -filter are given by

$$\frac{dx_1}{dt} = A_1x_1 + B_1v_i \quad (6) \quad y_1 = C_1x_1 \quad (7)$$

where the state matrix A_1 , input matrix B_1 , and output matrix C_1 are defined in the appendix.

E. L-Filter Model

A reduced model is required to model the L -filter. Since the converter- and grid-side currents are synonymous for the L -filter, the state vector can be expressed in terms of the converter current and grid voltage as

$$x_2 = [i^T \ v_g^T]^T. \quad (8)$$

With the input and output vectors defined as for the LCL -filter, the continuous-time state and output equations of the L -filter are given by

$$\frac{dx_2}{dt} = A_2x_2 + B_2v_i \quad (9) \quad y_2 = C_2x_2 \quad (10)$$

where the state matrix A_2 , input matrix B_2 , and output matrix C_2 are defined in the appendix.

III. MODEL PREDICTIVE DIRECT CURRENT CONTROL

MPDCC was first proposed in [8] and developed more formally in [1], [2], with an MV induction machine drive used as the case study. MPDCC takes the place of both the inner control loop and the modulator of a conventional Pulse Width Modulation (PWM)-based setup, and as such directly sets the switching states of the converter.

A. Control Problem

The aim of MPDCC is to regulate each of the output currents (in this case, the converter currents) within a set hysteresis bounds of width δ_i . The bounds are defined about the current references in the abc -frame, such that $|i_{rip,abc}| \leq \delta_i$, where the ripple current is defined as $i_{rip,abc} = i_{abc} - i_{abc}^*$. Total Demand Distortion (TDD), which expresses the sum of the harmonic currents as a percentage of the nominal fundamental current [1], is used to measure harmonic distortion. Because an NPC converter is used, the controller must also keep the neutral point potential within a set of hysteresis bounds of width δ_{NP} about the neutral point reference $v_n^* = 0$.

In addition to regulating the output variables, MPDCC aims to minimise the switching losses of the converter. This can be

achieved indirectly, by minimising the converter switching frequency, or directly, by estimating and minimising the converter switching loss.

B. Internal Model of the Controller

In order for the controller to predict future states and outputs, a discrete-time model of the system is needed. The discrete-time input vector $u(k)$ is most easily defined for both the LCL - and L -filter models in terms of the converter switch positions $u_{abc}(k)$

$$u(k) = [u_a(k) \ u_b(k) \ u_c(k)]^T \quad (11)$$

whilst the overall state vectors are appended to include the neutral point potential $v_n(k)$

$$x_1(k) = [i(k)^T \ i_g(k)^T \ v_c(k)^T \ v_g(k)^T \ v_n(k)]^T \quad (12)$$

$$x_2(k) = [i(k)^T \ v_g(k)^T \ v_n(k)]^T \quad (13)$$

as are the output vectors

$$y_1(k) = y_2(k) = [i(k)^T \ v_n(k)]^T. \quad (14)$$

By combining the models of the NPC converter and filter(s), and applying forward-Euler or exact discretization, an internal control model, which relates the discrete-time input vector to the state and output vectors, can be derived. Details regarding the derivation of such a model are provided in [1], [9], [10].

C. MPDCC Control Procedure

Beginning at the current time-step k , the MPDCC algorithm predicts the trajectories of the states and outputs forward in time for all admissible future switching sequences. At each step of the prediction, each sequence must remain a *candidate*. A candidate sequence is one for which each output is either *feasible* (within its bounds), or *pointing in the proper direction* (outside its bounds, but moving closer to them). If a sequence ceases to remain a candidate, then it is discarded.

The set of admissible sequences is controlled by a fixed *switching horizon*, N_s . The switching horizon is made up of the elements 'S' (switch) and 'E' (extend), as well as an optional 'e' element, which can be added as a prefix to the switching horizon. Each 'S' event represents a 'branch' on the tree of possible future switching sequences. Each 'e' or 'E' event represents an extension of the outputs, with the switching state frozen until one or more of the outputs cannot be extended any further. The fixed switching horizon gives rise to a *prediction horizon*, N_p , of variable length. The prediction horizon denotes the number of time-steps that MPC looks into the future. Depending on the composition of N_s , the width of the hysteresis bounds, and the specific sequence of switching states, N_p may range from a few time-steps to several dozen time-steps. Lengthening the switching horizon gives rise to longer prediction horizons, which usually improves the performance of the system.

The MPDCC algorithm is based on a 'Last In First Out' stack model. At each time-step k , the algorithm computes the optimal input $u(k)$ according to the following process.

- 1) Initialise the stack with the root node, which consists of the previous switching state $u(k-1)$, the current state vector $x(k)$, and the switching horizon N_s . If the

first element of the horizon is an 'e', duplicate the root node and add it to the stack, discarding the 'e' from the switching horizon of the top node.

- 2a) Take the top node with a non-empty switching horizon from the stack.
- 2b) Execute and remove the first element of the switching horizon. For 'S', branch on all feasible switching transitions. For 'E', extend the trajectories while holding the switching state constant, using either the internal control model or an interpolation or extrapolation technique [11].
- 2c) If a sequence is a candidate, add it to the top of the stack to form a new node. If not, discard it.
- 2d) If there are no nodes on the stack with non-empty switching horizons, stop. This results in predicted switching sequences $U^i(k) = [u^i(k), u^i(k+1), \dots, u^i(k+N_p^i-1)]$, where $i \in \mathcal{I}$ and \mathcal{I} is an index set, along with the corresponding state and output trajectories. Otherwise, return to 2a).
- 3) Compute the cost for each candidate sequence. This is given by

$$c^i = \frac{1}{N_p^i} \sum_{\ell=k}^{k+N_p^i-1} \|u^i(\ell) - u^i(\ell-1)\|_1 \quad (15)$$

for minimisation of switching frequency, or

$$c^i = \frac{E^i}{N_p^i} \quad (16)$$

for minimisation of switching losses. Here E is the total switching loss over the prediction horizon. A detailed description of the calculation of switching losses is given in [12].

- 4) Determine the switching sequence with the minimal cost

$$i = \arg \min_{i \in \mathcal{I}} c^i. \quad (17)$$

- 5) Apply the switch position $u(k) = u^i(k)$ and shift the horizon one step forward.

At the next time-step, the control algorithm is repeated with a new optimal switching state $u(k+1)$ determined. For further details regarding the formulation of the control problem and the MPDCC algorithm, the reader is referred to [1], [2].

IV. ACTIVE DAMPING STRATEGY FOR LCL -FILTER

The LCL -filter presents two resonant frequencies, which are given by

$$\omega_1 = \frac{1}{\sqrt{CL_g}} \quad (18) \quad \omega_2 = \frac{1}{\sqrt{C \frac{LL_g}{L+L_g}}} \quad (19)$$

where ω_1 is the frequency at which resonance between the converter- and grid-side currents occurs, and is therefore the frequency which requires damping. Passive damping resistors, as shown in Fig. 3, are a straightforward and effective way to reduce resonance. However, they are also inefficient, leading to substantial power loss.

Instead of using passive damping resistors, an Active Damping (AD) strategy based on the *Virtual Resistor* (VR) concept,

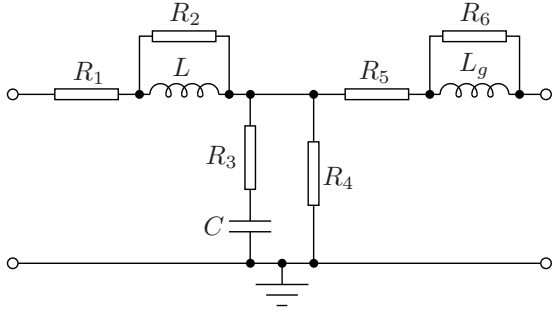


Fig. 3: Possible locations for passive damping resistors in an LCL -filter.

as outlined in [13], has been used. The VR strategy emulates the effect of a physical damping resistor(s) by modifying the converter current references with an additive damping component, which is calculated based on measured state variables at each time-step k .

An LCL -filter which includes a resistor R_4 in parallel with the capacitor can be modelled in block-diagram form as shown in Fig. 4(a) [13]. As shown in Fig. 4(b), which is the exact equivalent of the system in Fig. 4(a), the effect of R_4 can be realised by adding the quantity $-v_c/R_4$ to the converter current. The resistor R_4 can therefore be emulated by adding the damping quantity

$$i_{vr}^*(k) = \frac{-v_c(k)}{R_{v4}} \quad (20)$$

to the converter current reference at each time-step k , where $i_{vr}^*(k) = [i_{vr,\alpha}^*(k) \ i_{vr,\beta}^*(k)]^T$ and R_{v4} is the value of the VR emulating R_4 . The damping quantities which realise the effects of $R_1 - R_3$ and $R_5 - R_6$ can be similarly derived. The damping quantity $i_{vr}^*(k)$ is subsequently converted from the $\alpha\beta$ -frame to the dq -frame using the transformation

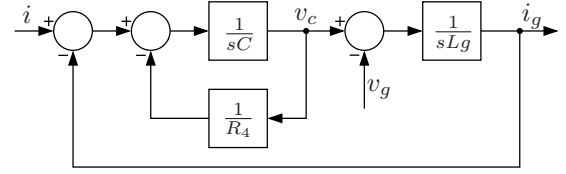
$$i_{vr,dq}^*(k) = K(\theta_k) i_{vr}^*(k) \quad (21)$$

where $i_{vr,dq}^*(k) = [i_{vr,d}^*(k) \ i_{vr,q}^*(k)]^T$, θ_k is the angle of the grid voltage at time-step k , and $K(\theta)$ is the transformation matrix

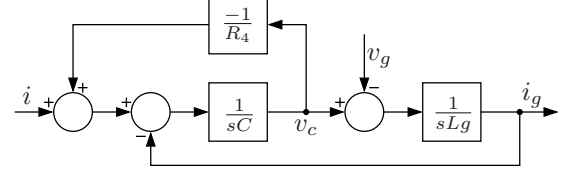
$$K(\theta) = \begin{bmatrix} \cos(\theta) & \sin(\theta) \\ -\sin(\theta) & \cos(\theta) \end{bmatrix}. \quad (22)$$

After removing the DC component of $i_{vr,dq}^*(k)$ using a High-Pass Filter (HPF), it is added to the fundamental reference $i_{f,dq}^*(k) = [i_{f,d}^*(k) \ i_{f,q}^*(k)]^T$ to give the overall dq converter current reference $i_{dq}^*(k) = [i_d^*(k) \ i_q^*(k)]^T$.

Because the MPDCC algorithm looks a number of time-steps into the future, it is necessary to update the damping quantity, and therefore current reference, over the course of the prediction. Rather than updating the reference at each time-step of each prediction, which adds significantly to the complexity of the algorithm, the reference is instead updated whenever the algorithm executes an 'S' event. The updated reference is calculated in the same manner as at time-step k , based on the predicted capacitor voltage $v_c(\ell)$ and the predicted angle of the grid voltage θ_ℓ , where ℓ is an arbitrary future time-step at which an 'S' event occurs. Note that if the horizon does not begin with an 'e', then updating the damping quantity is redundant for the first 'S' of the switching horizon,



(a) Direct representation.



(b) Equivalent representation.

Fig. 4: s -domain block diagram representations of an LCL -filter with a damping resistor R_4 in parallel with the filter capacitor C .

which naturally occurs at time-step k .

V. PERFORMANCE EVALUATION

A. Case Study

The performance of the proposed control strategy has been evaluated through a MATLAB-based simulation. The semiconductor models are based on the ABB 35L4510 4.5kV 4 kA Integrated Gate Commutated Thyristor (IGCT) and the ABB 10H4520 fast recovery diode. The LCL -filter parameters are $L = L_g = 600 \mu\text{H}$, both with a series resistance $R = R_g = 5 \text{ m}\Omega$, whilst the filter capacitor is $C = 1 \text{ mF}$. The resulting resonant frequency is $\omega_1 = 1290 \text{ rad/s}^{-1}$ (205 Hz). The L -filter parameters are $L = 1.2 \text{ mH}$, with a series resistance $R = 10 \text{ m}\Omega$, meaning that the overall resistance and inductance of the filter is the same for both cases. This also means that the losses in the LCL - and L -filters are approximately equal.

The per-unit system, which is used in all simulations, is established from foundation values of $V_{base} = \sqrt{2}/3V_g = 2449 \text{ V}$, $P_{base} = 8 \text{ MVA}$ and $f_{base} = 50 \text{ Hz}$. A summary of nominal ratings and per-unit (p.u.) parameters is shown in Table I.

All MPDCC simulations have been run with a sampling time of $25 \mu\text{s}$ and with the cost function penalising switching losses. Exact (model-based) extension has been used. The neutral point bound width $\delta_{NP} = 0.03 \text{ p.u.}$ and the virtual resistance $R_{v4} = 0.7 \text{ p.u.}$ For both the LCL - and L - filters the fundamental converter current references are set to deliver 1 p.u. real power and 0 p.u. reactive power to the grid.

B. Steady-State Performance Evaluation

Figs. 5 and 6 show the grid current, grid current spectrum, neutral point potential, and switching pattern, for MPDCC

TABLE I: Nominal ratings (left) and p.u. parameters (centre and right) of the system.

Grid, LCL-Filter & L-Filter					
Grid voltage	3000 V	L, L_g	0.168 p.u.	L	0.336 p.u.
Grid current	1540 A	R, R_g	0.004 p.u.	R	0.008 p.u.
Grid frequency	50 Hz	C	0.353 p.u.		
Converter					
DC-link voltage	5200 V	C_{dc}			3.534 p.u.
Apparent power	8 MVA				

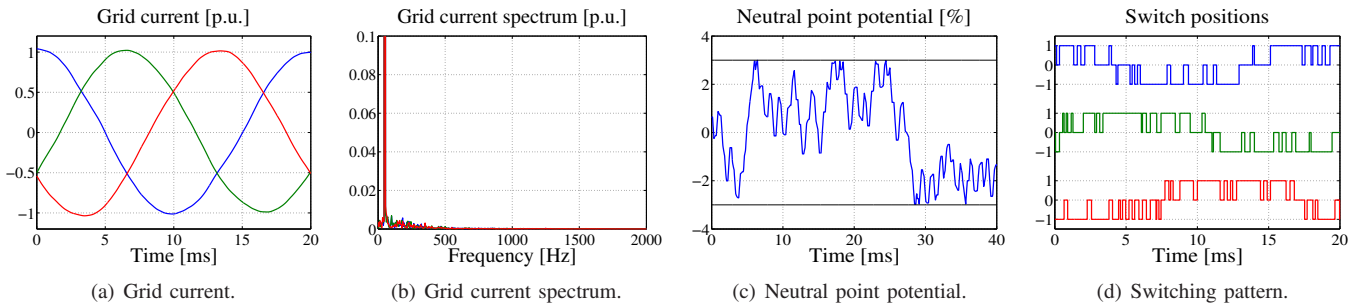


Fig. 5: Steady-state grid current, grid current spectrum, neutral point potential, and switching pattern, for MPDCC with an *LCL*-filter and active damping.

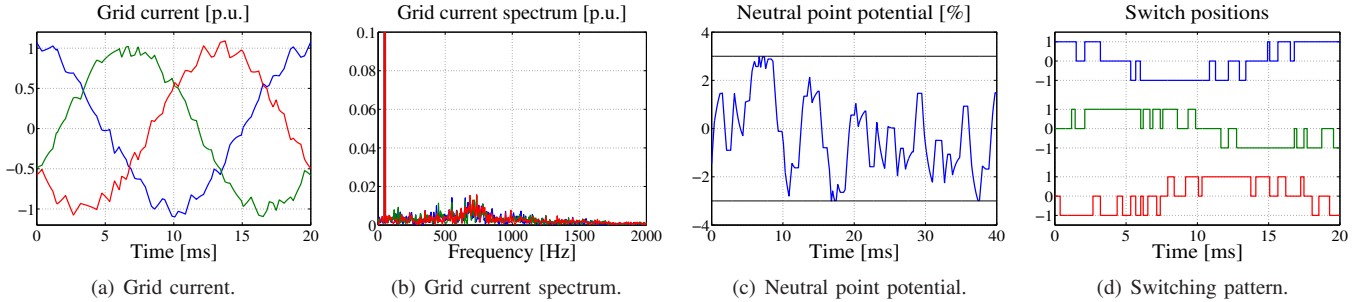


Fig. 6: Steady-state grid current, grid current spectrum, neutral point potential, and switching pattern, for MPDCC with an *L*-filter.

with an *LCL*- and *L*-filter, respectively. In both cases, the bound width $\delta_i = 0.1$ p.u. and the switching horizon $N_s = \text{'eSE'}$. For the *LCL*-filter, the resulting average device switching frequency is 548 Hz, average device switching losses are 33.9 kW, and grid current TDD is 2.13%. As shown in Fig. 5(b), the AD strategy is very effective in suppressing the resonant frequency ω_1 from the grid current. For the *L*-filter, the switching frequency is 262 Hz, the switching losses are 17.1 kW, and the grid current TDD is 7.10%.

The substantial discrepancy in switching frequency and losses is caused by the fact that the dynamics of the controlled (converter-side) current of the *LCL*-filter are much faster than those of the *L*-filter. For the *LCL*-filter, the inductance through which the converter-side current flows is only half that of the *L*-filter, and as a result the switching frequency is roughly double that of the *L*-filter. As shown in Figs. 5(c) and 6(c), the ability of the controller to balance the neutral-point potential is not affected by the introduction of the *LCL*-filter.

The increase in switching losses is offset by the considerable increase in harmonic attenuation offered by the *LCL*-filter, which results in a much lower grid current TDD. The trade-off between switching losses and grid current TDD is therefore a very important consideration and forms the basis of comparison between MPDCC with an *LCL*- and *L*-filter.

Fig. 7 provides trade-off curves showing grid-current TDD ($i_{g,TDD}$) against average device switching losses (P_{sw}). The comparison is made for switching losses of between 20 and 30 kW, and up to a grid current TDD of 5%, which is the maximum allowable grid current TDD according to the IEEE Standard 519 on harmonic limits. The data points are generated by varying the width of the current bound, δ_i , and a hyperbolic trendline is subsequently fitted.

Fig. 7(a) shows the trendlines for MPDCC with $N_s = \text{'eSE'}$. It is apparent that the performance of MPDCC with an *LCL*-

filter is superior to that with an *L*-filter at most values of P_{sw} . It is only below $P_{sw} = 22$ kW that the performance of the *L*-filter is better than that of the *LCL*-filter, at which point the TDD for both cases approaches 5%.

The trendlines with the switching horizon extended to 'eSESE' are shown in Fig. 7(b). Once again, the performance with an *LCL*-filter is superior to that with an *L*-filter when the switching losses are above roughly 22 kW. It is interesting to note that with the *LCL*-filter, the performance with $N_s = \text{'eSESE'}$ does not improve greatly over $N_s = \text{'eSE'}$, whilst with the *L*-filter, there is a substantial improvement. This means that for $N_s = \text{'eSESE'}$ the improvement offered by the *LCL*-filter over the *L*-filter is not as significant as with the shorter horizon.

Fig. 7(c) shows the trendlines with the switching horizon further extended to 'eSSESE'. With this horizon, the performance of MPDCC with an *LCL*-filter is considerably better than with an *L*-filter. At $P_{sw} = 20$ kW, the *LCL*-filter offers a grid current TDD of around 4.2%, compared to around 4.8% for the *L*-filter, whilst at $P_{sw} = 30$ kW, the *LCL*-filter offers a TDD of less than 2%, compared to around 3% for the *L*-filter.

The simulation results validate the effectiveness of the modified MPDCC strategy for use with an *LCL* output filter. At all of the switching horizons examined - 'eSE', 'eSESE', and 'eSSESE' - the modified strategy has been shown to outperform conventional MPDCC with an *L*-filter across a range of operating points. With switching horizons of 'eSE' and 'eSESE', the modified strategy performs worse than conventional MPDCC when the switching losses are below about 22 kW. However, this could potentially be corrected by further optimising the *LCL*-filter design. Moreover, modifications to the AD strategy, for instance the formulation of the damping quantity in (20), could also improve performance.

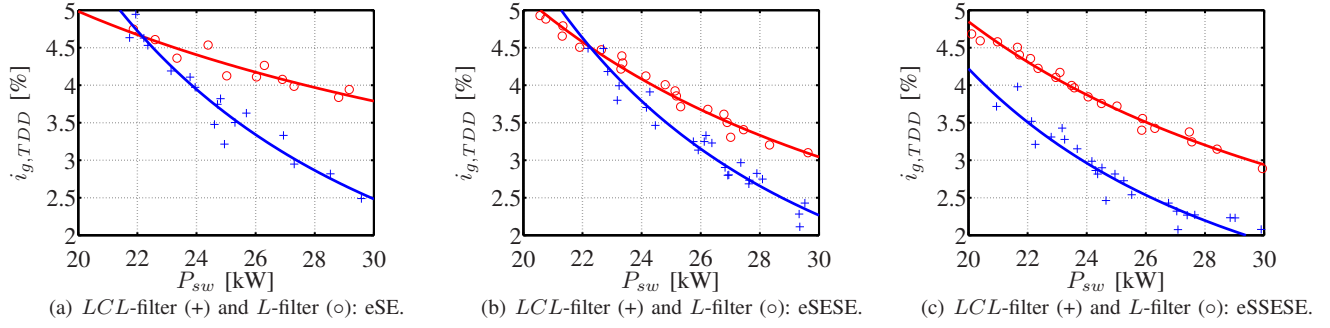


Fig. 7: Performance trade-off curves for MPDCC with an LCL - and L -filter. The plots show grid current TDD ($i_{g,TDD}$) against average device switching losses (P_{sw}).

VI. CONCLUSION

This paper has presented a modified MPDCC strategy for the control of a three-phase grid-connected NPC converter with an LCL -filter, which has been benchmarked against conventional MPDCC with a direct grid-connection (L -filter). The system has been modelled with both the LCL - and L -filters considered, and an overview of the MPDCC algorithm was provided. The active damping strategy, which is based on the virtual resistor concept, has been outlined, and through simulation it has been shown that the modified MPDCC strategy with an LCL -filter is able to offer a substantial improvement over conventional MPDCC with an L -filter. The benefit of the LCL -filter has been demonstrated for multiple switching horizons and across a range of operating points. Future work will include experimental verification of the proposed strategy.

ACKNOWLEDGEMENT

This work was supported by The University of Auckland Doctoral Scholarship.

APPENDIX

The matrices of the state-space models (6) - (7) and (9) - (10) are as follows

$$A_1 = \begin{bmatrix} \frac{-R}{L} & 0 & 0 & 0 & \frac{-1}{L} & 0 & 0 & 0 \\ 0 & \frac{-R}{L} & 0 & 0 & 0 & \frac{-1}{L} & 0 & 0 \\ 0 & 0 & \frac{-R_g}{L_g} & 0 & \frac{1}{L_g} & 0 & \frac{-1}{L_g} & 0 \\ 0 & 0 & 0 & \frac{-R_g}{L_g} & 0 & \frac{1}{L_g} & 0 & \frac{-1}{L_g} \\ \frac{1}{C} & 0 & \frac{-1}{C} & 0 & 0 & 0 & 0 & 0 \\ 0 & \frac{1}{C} & 0 & \frac{-1}{C} & 0 & 0 & 0 & 0 \\ 0 & 0 & 0 & 0 & 0 & 0 & 0 & -\omega \\ 0 & 0 & 0 & 0 & 0 & 0 & \omega & 0 \end{bmatrix} \quad (23)$$

$$B_1 = \begin{bmatrix} \frac{1}{L} & 0 & 0 & 0 & 0 & 0 & 0 & 0 \\ 0 & \frac{1}{L} & 0 & 0 & 0 & 0 & 0 & 0 \end{bmatrix}^T \quad (24)$$

$$C_1 = \begin{bmatrix} 1 & 0 & 0 & 0 & 0 & 0 & 0 & 0 \\ 0 & 1 & 0 & 0 & 0 & 0 & 0 & 0 \end{bmatrix} \quad (25)$$

and

$$A_2 = \begin{bmatrix} -\frac{R}{L} & 0 & -\frac{1}{L} & 0 \\ 0 & -\frac{R}{L} & 0 & -\frac{1}{L} \\ 0 & 0 & 0 & -\omega \\ 0 & 0 & \omega & 0 \end{bmatrix} \quad (26)$$

$$B_2 = \begin{bmatrix} \frac{1}{L} & 0 & 0 & 0 \\ 0 & \frac{1}{L} & 0 & 0 \end{bmatrix}^T \quad (27)$$

$$C_2 = \begin{bmatrix} 1 & 0 & 0 & 0 \\ 0 & 1 & 0 & 0 \end{bmatrix}. \quad (28)$$

REFERENCES

- [1] T. Geyer. Model predictive direct current control: Formulation of the stator current bounds and the concept of the switching horizon. *IEEE Ind. Appl. Mag.*, 18(2):47–59, Mar. 2012.
- [2] T. Geyer. A comparison of control and modulation schemes for medium-voltage drives: Emerging predictive control concepts versus PWM-based schemes. *IEEE Trans. Ind. Appl.*, 47(3):1380–1389, May/June. 2011.
- [3] N. Abdel-Rahim and J.E. Quaicoe. Modeling and analysis of a feedback control strategy for three-phase voltage-source utility interface systems. In *Proc. IEEE Ind. Appl. Soc. Meeting*, pages 895 – 902, Denver, USA, Oct. 1994.
- [4] E. Twining and D.G. Holmes. Grid current regulation of a three-phase voltage source inverter with an LCL input filter. *IEEE Trans. Power Electron.*, 18(3):888 – 895, May 2003.
- [5] P.C. Loh and D.G. Holmes. Analysis of multiloop control strategies for LC/CL/LCL-filtered voltage-source and current-source inverters. *IEEE Trans. Ind. Appl.*, 41(2):644 – 654, Mar./Apr. 2005.
- [6] L.A. Serpa, S.D. Round, and J.W. Kolar. A virtual-flux decoupling hysteresis current controller for mains inverter systems. *IEEE Trans. Power Electron.*, 22(5):1766 – 1777, Sep. 2007.
- [7] L.A. Serpa, S. Ponnaluri, P.M. Barbosa, and J.W. Kolar. A modified direct power control strategy allowing the connection of three-phase inverters to the grid through LCL filters. *IEEE Trans. Ind. Appl.*, 43(5):1388 – 1400, Sep./Oct. 2007.
- [8] J. C. Ramirez Martinez, R. M. Kennel, and T. Geyer. Model predictive direct current control. In *Proc. IEEE Int. Conf. Ind. Techn.*, pages 1808 – 1813, Vina del Mar, Chile, Mar. 2010.
- [9] T. Geyer, G. Papafotiou, and M. Morari. Model predictive direct torque control - part I: Concept, algorithm and analysis. *IEEE Trans. Ind. Electron.*, 56(6):1894–1905, Jun. 2009.
- [10] T. Geyer, J. Scoltock, and U. Madawala. Model predictive direct power control for grid-connected converters. In *Proc. IEEE Ind. Electron. Soc. Conf.*, pages 1438 – 1443, Melbourne, Australia, Nov. 2011.
- [11] Y. Zeinaly, T. Geyer, and B. Egardt. Trajectory extension methods for model predictive direct torque control. In *Proc. IEEE Appl. Power Electron. Conf. Expo.*, pages 1667 – 1674, Fort Worth, USA, Mar. 2011.
- [12] T. Geyer. Generalized model predictive direct torque control: Long prediction horizons and minimization of switching losses. In *Proc. IEEE Conf. Decis. Control*, pages 6799 – 6804, Shanghai, China, Dec. 2009.
- [13] P.A. Dahono. A control method to damp oscillation in the input LC filter of AC-DC PWM converters. In *Proc. IEEE Power. Electron. Spec. Conf.*, pages 1630 – 1635, Cairns, Australia, Jun. 2002.